Lorentz Force Accelerator with an Open-ended Lithium Heat Pipe *

E.Y. Choueiri†, V. Chiravalle‡, George E. Miller§
& Robert G. Jahn¶
Electric Propulsion and Plasma Dynamics Laboratory (EPPDyL)
MAE Dept.
Princeton University, Princeton NJ 08544.

W. Anderson & J. Bland
Thermacore Inc., Lancaster, PA

AIAA-96-2737‖

Abstract

A steady-state coaxial Lorentz force accelerator (LFA), where lithium propellant is supplied by an open-ended heat pipe, was designed and built. The open-ended heat pipe provides a novel alternative to the complex propellant feeding systems previously used with lithium-fed thrusters. The closed end of the heat pipe acts as a reservoir containing a liquid lithium pool, and a wick. The main part of the pipe is embedded in a furnace (1200° C) which vaporizes the lithium off the wick. The lithium vapor then travels to the open end which is also the cathode of the LFA supplying the propellant for the plasma thruster. The actively heated cathode is a hybrid hollow-multi-channel cathode consisting of 48 longitudinal channels embedded in a porous tungsten insert. The design promises a substantial decrease in the erosion rate of the cathode which is the lifetime limiting component in such thrusters. This paper describes the design and fabrication of the thruster as well as the mass flow rate calibration procedure which relies on careful water calorimetry.

*This work is supported through an SBIR contract from NASA-JPL.

†Chief Investigator at EPPDyL. Assistant Professor, Applied Physics Group. Senior Member AIAA.

‡Student supported by the New Jersey NASA Space Grant Consortium.

§System Engineer, EPPDyL.

¶Professor of Aerospace Sciences. AIAA Fellow.

‖Presented at the 32^{nd} AIAA Joint Propulsion Conference.

1 Introduction

1.1 long lifetime and high efficiency of Li LFA's

The lithium-fed Lorentz force accelerator (LFA) is a variant of the magnetoplasmadynamic thruster (MPDT) that promises long lifetime (>1000 hrs) and high efficiency (>60%). The extension of the lifetime of such thrusters to above 1000 hours through the use of lithium as propellant in multi-channel cathodes has been recently shown to be within reach[1], thus overcoming the main obstacle in the use of such thrusters for spacecraft propulsion.

This substantial lifetime extension is due to the the role of lithium in lowering the effective work function ϕ of the cathode (pure tungsten's $\phi \simeq 4.5$ eV while pure lithium's $\phi \simeq 2.9$ eV) and the role of the multi-channels in lowering the current densities, thus allowing lower operating surface temperatures, for a given total current, and consequently far lower erosion rates through evaporation. Evaporation has been shown to be the major erosion mechanism in steady-state MPDT's.

It is now also well known[2] that another advantage of the use of alkali metal propellant is the superior thrust efficiencies which have been reported to well exceed 60%. This is believed to be related to the scaling of the energy sink associated with ionization (first ionization potential, ϵ_i, for lithium is 5.4 eV while ϵ_i=15.8 eV for argon.) This is especially the case since ionization is believed to be of anomalously

high importance in such devices[3].

The only remaining concern for using the lithium LFA on actual spacecraft is the contamination issue. In 1990 an experiment was conducted on the Soviet spacecraft Progress M-4, specifically to study, using the quartz microbalance technique, spacecraft contamination from alkali metal plasma sources. The results of that experiment were recently published and discussed by Brukhty et. al.[4], who also presented further experimental and theoretical results and concluded that the deposition of alkali metals on spacecraft is not an obstacle for utilizing them as propellant in electric thrusters. Furthermore, recent numerical simulations[5] for a lithium MPD thruster have shown that plume shields can be quite effective in reducing the backflow of lithium to the spacecraft.

1.2 Advantages and Applications of Li LFA's

Among all candidate electric propulsion options, the Li LFA has the unique capability of offering extremely high thrust densities (10^2 to 10^5 N/m^2). This feature, the LFA's ability of processing very high power (10^4 to 10^7 W) through a small, compact and simple device, and its high specific impulse (1000-4000 s) put it in a class by itself for application to many thrust-intensive and energetic missions such as demanding cargo and piloted planetary missions. For more power-limited near-term applications the LFA could also compete with other EP options especially for applications such as orbit-raising of massive payload.

Since the Li LFA becomes adequately efficient (>30%) only at higher power level (>30 KW) (see Ref. [6] for instance) and since no such high power sources are available in space, the device has been classified in the US as an "advanced propulsion option."

1.3 NASA-sponsored research on the Lithium LFA

NASA-JPL's research program on Li LFA's is concentrated primarily on demonstrating engine performance in a 100 kW-class thruster and proving the feasibility of long-lived, high current cathodes. The program includes the following complementary activities:

1. The fabrication and testing of a 100 kW Li LFA at the Moscow Aviation Institute[7] with the goal of demonstrating an efficiency of 40-45% at an I_{sp} of 3500-4000 s.

2. In-house work at JPL aimed at the development of a cathode thermal code incorporating models of the heat fluxes from the near-cathode plasma and testing at high current levels to validate the code[8]. The experiments include number density measurements using the Pulsed Electron Beam diagnostic developed at USC.

3. Development and testing of a 30 kW class Li LFA through a collaboration between Thermacore Inc. and Princeton University's EPPDyL

4. Experimental and theoretical studies of the fundamental aspects of multi-channel cathodes for Li LFA's at Princeton University.

While previous work with lithium plasma thrusters at EPPDyL[9, 10, 11] concentrated on a "proof of concept" studies of the benefits of lithium and barium dispenser cathodes, the new thruster described in this paper is intended for more extensive and fundamental studies under realistic LFA conditions.

Among the advanced diagnostics especially developed for these experiments, is a high resolution six color video pyrometer (SCVP) (described in ref. [12]) for measuring the high surface temperature of LFA components without knowing their emmisivities.

1.4 Paper Organization

This paper describes the design, development and implementation of the Li LFA, that is being used for the studies in Programs 3 and 4 (listed above). In Section 2 the design is presented with particular emphasis on the novel aspect of the device, namely its use of an open-ended heat pipe to deliver a metered flow of lithium without the complexity of previous and existing systems elsewhere. In Section 3 we present a description of the LFA Testing Facility. The mass flow calibration and monitoring, which rely on careful water calorimetry, are presented in Section 4 where the experimental results of the calibration are also discussed. Finally, in the appendix we discuss a theoretical fluid/thermal model of the lithium flow that was helpful in guiding the mass flow calibration.

2 Design of an LFA with a lithium Open-Ended Heat Pipe

2.1 General Description

A cross-sectional schematic of the design is shown in Fig. (1). The drawing shows the dimensions of the component and traces the flow of lithium through the heat pipe that acts as the propellant reservoir. A 3-D schematic of the LFA is shown in Fig. (2).

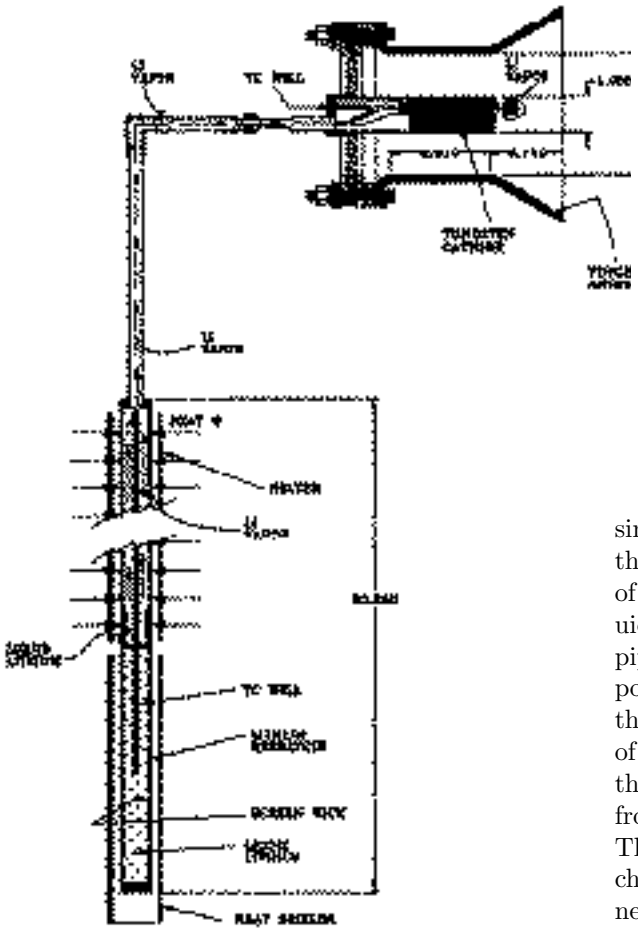

Figure 1: Cross-sectional schematic of the accelerator showing dimensions (in inches) and the flow of lithium vapor.

The open-ended heat pipe provides a novel alternative to the complex propellant feeding systems previously used with lithium-fed thrusters. Aside from

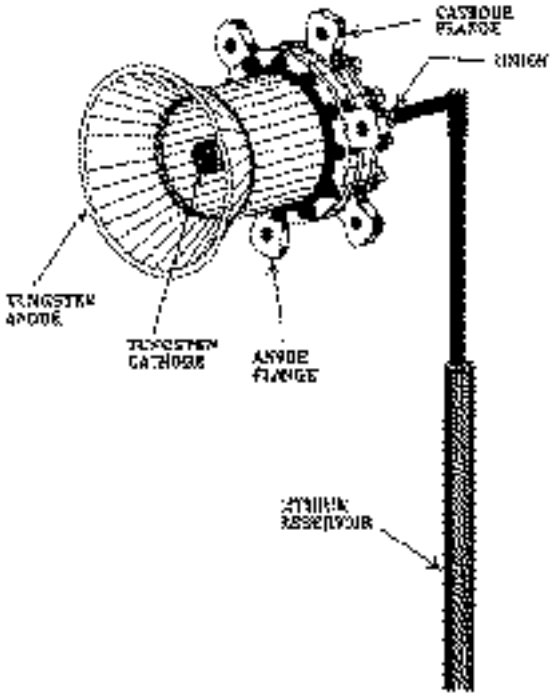

Figure 2: 3-D schematic of the accelerator.

simplicity, reliability is enhanced by the fact that there are no valves or moving parts. The closed end of the heat pipe acts as a reservoir containing a liquid lithium pool, and a wick. The main part of the pipe is embedded in a furnace (1200° C) which vaporizes the lithium off the wick. The lithium vapor then travels to the open end which is also the cathode of the LFA supplying the propellant for the plasma thruster. Capillary forces draw up additional lithium from the reservoir to replace the vaporized lithium. The actively heated cathode is a hybrid hollow-multichannel cathode consisting of 48 longitudinal channels embedded in a porous tungsten insert.

Rationale for the vaporizer design. The vaporizer design of the reservoir was deemed superior to a pool boiler for our particular application. Compared with more conventional fluids, alkali metals have high nucleation superheats, high bubble growth rates, long waiting times between bubble nucleations, and high natural convection rates. These conditions can cause problems with unstable boiling and with

incipient boiling superheats. In unstable boiling, the heat transfer mechanism oscillates between nucleate boiling and liquid natural convection, sometimes resulting in violent shaking of the system. The vaporizer design eliminates potential pool boiling problems.

Some of the more important design parameters of the system are listed in Table 1.

The thruster is radiatively cooled and does not have an applied magnetic field. Although an applied magnetic field has been shown to substantially improved the performance[7], we will be operating the thruster in a self-field mode for our fundamental studies. Future performance study would necessitate an applied field.

Thermocouples wells were placed in three critical locations (labeled TC in Figure 1) to provide access for temperature measurement at 1) the middle height of the canister (where the evaporation takes place), 2) the top of the canister and 3) the root of the cathode.

2.2 Cathode Design Considerations

A multi-channel configuration, that has the promise to yield a larger effective attachment area and also, a more stable behavior of the discharge, was chosen. The elementary channel packet is slightly recessed with respect to the cathode end (about 25% of the inner diameter). This hybrid hollow-multichannel cathode configuration[13], should combine the advantages of both, a movement of the discharge into the cavity (as in the hollow cathode) and a larger emitting surface (as in the multi-hollow cathode).

According to a great deal of literature, and also to some experiments carried out at EPPDyL[14], the penetration length of the discharge is typically on the order of a few channel diameters. Considering that in a multichannel cathode this length is greatly reduced with respect to a single channel cathode with the same hollow cross section area and the same total gas flow rate, we expect that a length of 5 cm for the insert containing the channels, is widely in excess of any possible penetration of the discharge.

Considering the ratio of the total discharge current to the cathode cross section area (without the outer sheath), we predict a current density not larger than 260 A/cm^2. This is about the same value as the thruster in ref. [1]. If we maintain the same ratio of hollow cross-section area to the total area (about 13%), using gaps of 2 mm diameter tungsten rods, as in ref. [1], and cylindrical holes in the tungsten wick, it follows that sixty-five uniformly spaced 1 mm diameter channels are needed, having cross section (0.78 mm^2) with gaps of (0.16 mm^2).

2.3 Anode Design Considerations[1]

From a machining and cost point of view, tantalum is preferable over tungsten for anode material. The design calculations presented below, however, favor the use of tungsten.

In order to choose the anode material and estimate the minimum anode thickness compatible with the operating conditions of the thruster, the effects of Joule heating, heat flux to the anode and spot attachments were considered.

2.3.1 Joule heating.

A simple model is considered, in which, once a steady state is reached, all power generated in the anode by resistive heating (Joule effect) is rejected by radiation. This model yields an expression for the anode thickness t,

$$t = \frac{I^2 \rho}{(2\pi R)^2 \epsilon \sigma T^4}. \tag{1}$$

where ρ is the resistivity of the material, ϵ is the total emissivity, σ is the Stefan-Boltzmann constant, T is the temperature in degrees K and I is the total current. Using temperature-dependent expressions for the resistivities of tungsten and tantalum, the melting temperatures of tungsten (3683 K) and tantalum (3269 K) and assuming an operating current of 1000 A, we obtain a minimum thickness equal to 3.5 μm for a tungsten anode and to 7.7 μm for a tantalum anode. These results, show that Joule effect is not a dominant mechanism in anode heating.

2.3.2 Heat Flux to the Anode

For nominal LFA operation the anode heat flux q can be estimated as:

$$q = \left(V_a + \frac{5}{2} \frac{k_B T}{e} + \phi_a \right) + P_R, \tag{2}$$

where j_e is the electron current density, V_a is the anode voltage fall, T_e is the electron temperature, k_B is the Boltzmann constant, e is the elementary electric charge, ϕ_a is the work function for the anode material and P_R is the power radiated from the cathode.

If we now assume that the discharge attaches uniformly to the flared part of the anode, which has an

[1]The calculations in this section were carried by Paolo Gessini at EPPDyL.

DESIGN OEPRATING PARAMETERS	
Nominal LFA Power Rating	10-100 kW
Nominal LFA Current Rating	300-2000 A
Nominal LFA Voltage	30-50 V
Nominal Li Flow Rate	2-50 mg/s
Furnace Power	1.2 kW
Potential Drop Near Cathode	5 V
Background Pressure	10^{-4} torr
Li Vapor Pressure Next to Active Surface	2 to 20 torr
Maximum Emitting Surface Temperature	3000° K
DIMENSIONS	
Cathode O.D.	2.54 cm
Anode O.D. at Exit	15 cm
Minimum Radii for Corners	.062
Number of Hollow Channels	48
MATERIAL	
Cathode and Anode	Tungsten
Cathode Insert	Porous Tungsten
Cathode & Anode Mounting Flanges	Molybdenum
Inter-Electrode Insulator Flange	Sapphire
Bolt Insulators	Alumina
Canister Envelope	Molybdenum
Vapor Tubes and Thermocouple Wells	Tantalum
Li RESRVOIR & FURNACE	
Reservoir Capacity	1000 cm^3
Furnace Operating Temperature	1500° C
Furnace Maximum Current	500 A
Furnace Maximum Voltage	10 V
Furnace Active Element	3×30 cm Tungsten ribbon
CATHODE HEATER	
Material	Tantalum wire & alumina beads
Length	2 m wrapped around base of cathode
Operating Temperature	1100° C
Power Requirements	20 A at 50 V

Table 1: Design Parameters of Lithium LFA.

area of 220 cm^2, from typical values of the above physical quantities measured during operation of a similar device, we estimate that q should not exceed 200 W/cm^2. If we further assume that, once a steady state is reached, only the external surface of the flared part of the anode is at a uniform temperature and radiates the power away, using the appropriate values for emissivity and neglecting the thickness of the anode, we obtain, at 1000 A, a temperature of about 3050° K for tungsten, and 3280° K for tantalum. This difference is due to the lower emissivity of tantalum (about 0.3 as opposed to about 0.4 of tungsten). We notice that, while with tungsten we are well below the melting point, with tantalum we are slightly above. Tungsten thus provides a far better safety margin.

2.3.3 Non-uniform discharge: spot attachment

We now consider the destructive effects of spot attachment whereas the discharge is not uniform over the whole anode surface, but concentrated in a finite number of spots of a certain diameter. In order to obtain a rough estimate of the temperature evolution in the anode, we will make a series of assumptions, based in part on the results of experiments carried out with a quasi-steady MPD thruster at EPPDyL [15] which will render our conclusions conservative.

We will assume, from observations of spot traces in an LFA anode, that the current is concentrated in spots with 1 mm^2 area, distributed on the anode surface with an average density of one spot per cm^2. This means that only 1% of the surface is affected by the discharge. For spot lifetime we will assume that a single spot does not exist in the same location for a time longer than 100 μs. Such an assumption, quite conservative, is based on noise data, which present a characteristic frequency on the order of 100 KHz and could be attributed to spot movement on the anode surface with a characteristic time of 10 μs.

Analytical Model. Under these assumptions, a first analysis has been carried out using a one-dimensional model. Namely, the anode has been treated like a semi-infinite body, with constant heat flux at the boundary. In this way, radiation cooling has been neglected, and the temperature increase may be written as:

$$\Delta T = \frac{2q}{k}\left[\left(\frac{\alpha t}{\pi}\right)^{\frac{1}{2}} e^{-x^2/4\alpha t} - \frac{x}{2}\mathrm{erfc}\frac{x}{2\sqrt{\alpha t}}\right], \quad (3)$$

where the heat flux q is now equal to 20000 W/cm^2, k is the thermal conductivity, α is the thermal diffusivity and erfc $= 1 -$ erf, where erf is the error function. Constant values have been assumed for density, thermal conductivity and specific heat. These two last quantities do actually show a strong dependence on temperature, but in our range of interest ($T \geq$3000 K) they both tend asymptotically to a constant value, with little variation, thus upholding our assumption. The results are shown in figure 3. We can see that

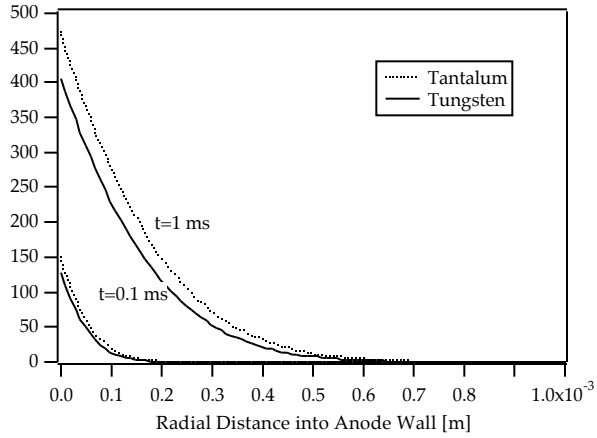

Figure 3: Temperature profiles at different times. Comparison between tantalum and tungsten

tungsten gives a slightly better performance than tantalum in that temperature is lower at the inner wall, but then it tends to become equal to that of tantalum toward the outer wall. This means that there will be a smaller possibility of overheating on the inside, and at the same time heat will be conducted equally efficiently out, where it will be radiated away by the external surface of the anode. From this simple model we see that, assuming a steady state operation temperature like the one previously estimated, say 3000° K, after 100 μs temperature is still below the melting point for both materials. In the case of tungsten, there is still no melting even after 1 ms.

Numerica Model. A more detailed picture of the effect may be obtained with a three-dimensional axisymmetric model including radiation. A 1 cm diameter disk, 2 mm thick, with a 1 mm diameter spot around its axis of symmetry on one side simulates the region of a 2 mm thick anode surrounding each single spot. The boundary conditions are $q =$ 20000W/cm^2 at the spot, $q = 0$ on the rest of the inner surface

and on the lateral area (for symmetry), $q = \epsilon\sigma T^4$ on the outer surface. The initial condition is a uniform temperature of 3000° K, and the properties of the material are again assumed constant, with the same values as before. Figure 4 shows the results of this simulation, performed with FEHT, a finite-element heat transfer program, in the case of tungsten. From

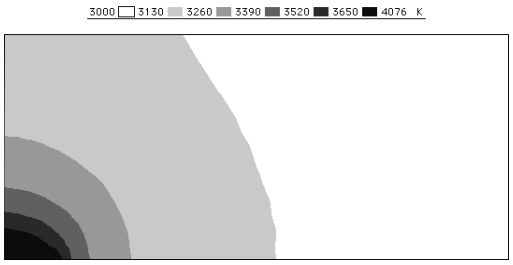

Figure 4: Temperature contours after 1.5 s in a 2 mm thick tungsten anode. The melting region is 13% of the anode thickness.

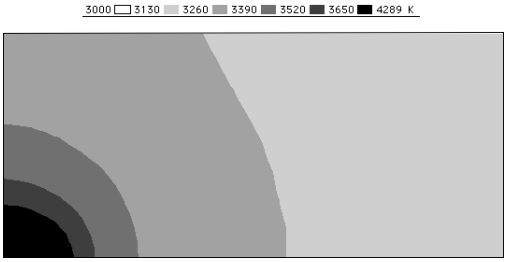

Figure 5: Temperature contours after 1.5 s in a 2 mm thick tantalum anode. The melting region is 100% of the anode thickness.

that plot we can note that even after 1.5 s, a period much longer than the expected lifetime of a spot, the region above the melting point extends for only about 13% of the anode thickness.

The same analysis, performed with tantalum, shows a less favorable behavior, with higher temperatures, mainly due to the lower emissivity of tantalum with respect to tungsten. For comparison, the same gray level scale has been used in figure 5.

Final Anode Selection As a result of the above design consideration a tungsten anode was manufactured by plasma spraying with a thickness of 4.5 mm

3 LFA Testing Facility

The Li LFA was installed in EPPDyL's Steady-State Low Power (SSLP) Facility described in ref. [10]. The SSLP facility uses a 1.5 m diameter cylindrical carbon steel tank, 6.4 m in length, evacuated to 10^{-5} torr by a set of mechanical and diffusion pumps. Photographs of the accelerator and furnace assembly with associated subsystems are shown in Figures 13 to 16. For the sake of clarity, the cathode heater was removed in these pictures.

In order to avoid contaminating the vacuum pumps with lithium, a condenser trap was built and positioned about 2.5 m downstream of the thruster. The trap consists of two copper plates actively cooled by chilled water coils and a similarly cooled metallic cylinder housing a mirror for optical diagnostic access (see Fig. (16)). In order to further protect the mirror from lithium condensation, its surface is kept at about 700° C using a small heater.

Data Acquisition. Data is recorded from sensors inside the vacuum tank using a Keithley System 570 digital acquisition board coupled to a personal computer. Aside from scientific diagnostics, three types of data are collected during a firing of the lithium-fed LFA , voltage and current data for the heater and the thruster both of which have separate power supplies, mass flow rate data of the reservoir cooling water and temperature data from thermocouples in the cooling water and in the walls of the canister.

Power Measurements. Current measurements are taken on the outside of the vacuum tank using magnetic current sensors from Bell Inc. The Keithley System 570 has 16 channels for differential voltage input. The uncertainty in a current value obtained from the sensor is quoted as 0.5 %. The heater input voltage is measured directly from the heater electrodes and the signal is passed through a voltage divider before being sent to the Keithley board. The thruster voltage is measured from the connections at the window interface.

Water Flow Measurements. A turbine cage flow meter from McMillan Company is used to measure the flow rate of cooling water into the heater cooling jacket. The cooling water flow rate is one of the parameters required for determining the lithium mass flow rate by the balance of power into the heater. The flow meter is powered by a 5 V DC power supply and the voltage output of the device is proportional to the

mass flow rate through the meter. A calibration was performed to find this relationship and the associated uncertainty.

Temperature Measurements. Two sets of thermocouples are used to make measurements of the temperature of the canister wall and the temperature of the cooling water. The thermocouples used to measure the water temperature are Iron-Constantan junctions. The iron and constantan wires that extend from the thermocouple junctions are connected directly to a thermocouple daughter board in the Keithley system. Reference junction voltage compensation is applied to the thermocouple voltage signals by a Keithley software routine which computes the temperature in °C at the thermocouple junction. Tungsten-Rhenium junctions are used to measure the temperature of the canister wall at distances of 0.0508 m and 0.1524 m from the top of the canister. Cold junction voltage compensators are connected to the high temperature thermocouple lines and the voltage output from each of these devices is sent to the Keithley board. A calibration relation supplied by the manufacturer is used to find the temperature in °C.

4 Mass Flow calibration

Originally, the intention was to use a tantalum bellows between the reservoir and the thruster. The mass flow rate of lithium would then be measured using a load cell underneath the lithium reservoir. The bellows manufacturer calculated that the .254 mm tantalum foil used in the bellows should give a very soft spring, unfortunately, the bellows were so stiff that they were unusable probably due to work hardening of the tantalum. Annealing the bellows was unsuccessful. A calorimetry-based mass flow rate calibration and monitoring system was consequently devised and implemented. This section describes these activities and presents the results of the calibrations.

A lithium flow simulation model, discussed in the appendix, was developed to estimate the dependence of the lithium mass flow rate on the canister temperature and to determine the useful operating temperature range of reservoir.

4.1 canister Thermal Measurements

A series of measurements were taken to determine the power radiated from the heater during steady-state operation. This was accomplished by heating the canister while it is sealed, i.e. the canister was disconnected from the thruster and sealed with a tantalum swagelock cap.

In the ideal case liquid lithium would evaporate from the screen wick and condense on the surface of the vapor tube, transferring heat from the canister to the vapor tube. The assumption is that the canister walls are heated uniformly so that there would be no condensation on the screen wick which covers the canister walls and all the lithium vapor condensation would take place on the walls of the vapor tube. This assumption does not truly hold for our actual canister because the tungsten heating element is about 5 cm shorter than the upper extent of the vertcal part of the canister and as a consequence the top part of the canister is not heated by the heating element. Therefore condensation of lithium vapor is expected in this region once the temperature in the lower part of the canister is sufficient for vaporization to take place. Under such conditions the canister behaves as a heat pipe with lithium as the working fluid. After condensing in the top part of the canister the liquid lithium flows along the screen wick toward the region of the canister that is actively heated and evaporation takes place again. The iron cooling jacket of the canister (see the photographs in Figures 15 and 16) does not cover the top part of the canister, and in this region the canister radiates as a greybody. The loss of radiated power from the walls of the vapor tube is eliminated through the use of alumina insulators and molybdenum foil that cover the vapor tube. The power lost to the tank due to greybody radiation of the canister is concentrated in the top part of the canister. The radiated power loss to the tank from the canister is an important parameter in determining the lithium mass flow rate using power balance methods. Two experiments were performed in which the power to the heater was gradually increased in steps and the thermal response of the canister was recorded. As mentioned earlier measurements of canister temperature were made with two thermocouples, one in the top part of the canister where there is no active heating from the tungsten element and one in the bottom part where there is active heating. The experiments were roughly four hours in duration each. Fig. 6 and Fig. 7 show the results of these experiments.

As Fig. 7 shows a temperature difference between the top and bottom thermocouples readings of about 200 deg C was observed during steady state with the bottom temperature at 700 deg C and the input power at 450 W. Once the vaporization threshold was reached the temperature gradient was reduced

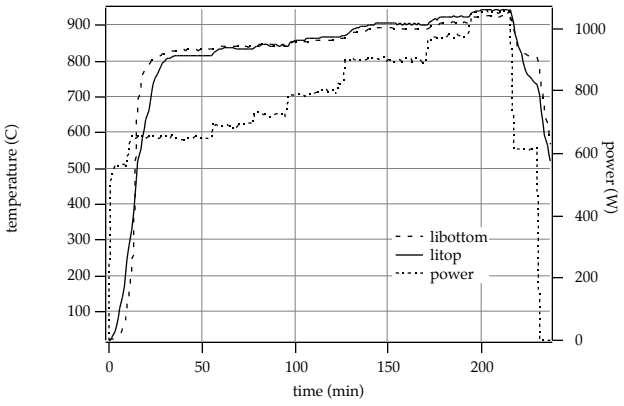

Figure 6: First canister thermal response experiment. Litop refers to the reading from the thermocouple that is closest to the top of the canister

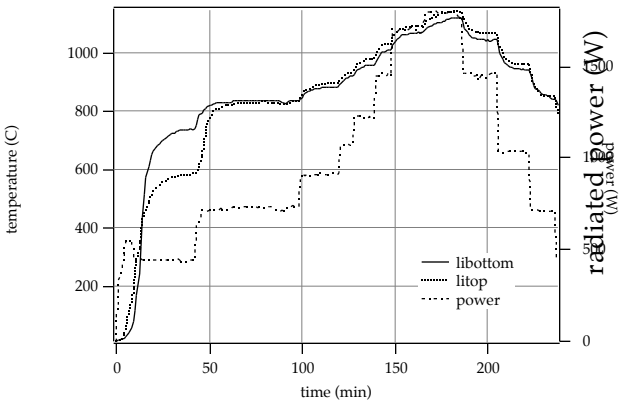

Figure 7: Second canister thermal response experiment. Litop refers to the reading from the thermocouple that is closest to the top of the canister

significantly. This observation supports the notion that the canister behaves like a heat pipe with a flat temperature profile. The measurements show that steady-state conditions were reached when thermocouple data was constant within 0.1% for a period of about three minutes. Cyclic variations in the input power to the heater from the power supply were observed with amplitude of 10 W. The power radiated to the tank during steady state was computed using the following equation.

$$P_{Rad} = P - \dot{m} c_p \Delta T \tag{4}$$

Here P is the input power to the heater computed from current and voltage measurements, $\dot{m}$ is the mass flow rate of water through the iron cooling jacket, and ΔT is the difference between the cooling water inlet and outlet temperatures. The values used in Eq. 4 were obtained by taking an average of three consecutive steady-state points. A standard deviation was also computed for each of the parameters in Eq. 4. An error propagation analysis was performed to find the uncertainly in the computed values of P_{Rad} from the uncertainties in its parameters. The values of P_{Rad} at several steady-state points taken from the two experiments are plotted in Fig. 8 versus T_{Top}^4 where T_{Top} is the the temperature at the top of the canister. A linear fit to the data yielded

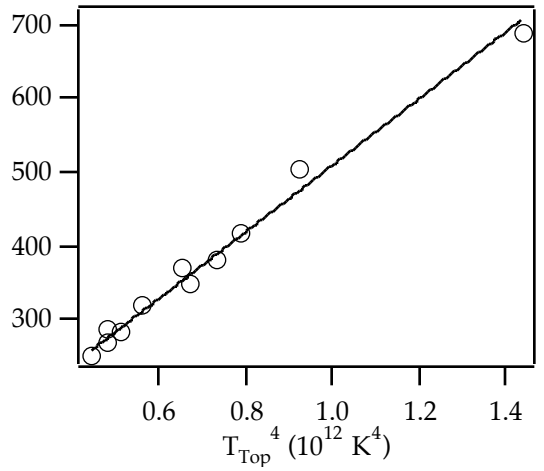

Figure 8: Radiated power from the canister as a function of T_{Top}^4

the following coefficients.

$$P_{Rad} = 57.7 + 4.52 \times 10_{-10} T_{Top}^4 \tag{5}$$

The variance of both of the coefficients above was computed to estimate the total error in the mass flow calibration.

4.2 Results of Li Mass Flow Calibration

The mass flow rate of lithium through the thruster during steady-state operation can be determined experimentally by considering the modes of heat transfer to a system comprising the heater and canister. Three of these modes were considered in the last section, the heat addition from the electrical resistance of the tungsten heating element, P, the heat loss from convection of the water through the iron cooling jacket and the heat loss from the greybody radiation of the top part of the canister, P_{Rad}. During thruster operation, an additional mode of heat loss during steady state is evaporation of lithium which can be expressed as the product of the latent heat of vaporization of lithium, Λ and the mass flow rate of lithium from the canister, $\dot{m}_{Li}$. We essentially measure the rate of heat loss through the evaporation of lithium and with the knowledge of Λ we determine $\dot{m}_{Li}$. Since the thruster cathode and the canister are directly connected by a tantalum vapor tube, conduction occurs from the cathode to the heater. The rate of heat transfer through this mode is calculated from the equation below.

$$q = \frac{\kappa A}{L}\delta T \tag{6}$$

Taking the temperature difference between the cathode and the canister to be 1000 °C, the cross sectional area of the vapor tube as 8.639×10^{-6} m, the thermal conductivity as 100 $\frac{W}{mK}$ and the length of the vapor tube as 0.5 m, the power supplied to the canister is only 1.72 W. This value is negligible compared with the other transfer modes and has been consequently neglected in the analysis.

Having identified the relevant modes of heat transfer, equating the power contributions from each of these modes leads to the follow expression relating the lithium mass flow rate to the other variables.

$$\dot{m}_{Li} = \frac{P - \dot{m}c_p\Delta T - P_{Rad}}{\Lambda} \tag{7}$$

Λ at the boiling point temperature (1 atm) of 1612.1 K is determined from an experimental vapor pressure curve for lithium in Ref. [16] and has the value of 21.62 $\times 10^6 \frac{J}{kg}$. The temperature dependence of Λ is found using the Watson relation described in Ref. [17] and has the form below.

$$\Lambda = 21.62 \times 10^6 \left(\frac{1 - \frac{T}{3503}}{1 - \frac{1612.1}{3503}}\right)^{0}.38 \tag{8}$$

Here 3503 °K is the critical temperature for lithium. The error in Eq. 7 is given by the following.

$$\sigma_{\dot{m}_{Li}} = \sqrt{\sigma_P^2 + (c_p\Delta T)^2\sigma_{\dot{m}}^2 + (\dot{m}c_p)^2\sigma_{\Delta T}^2 + \sigma_{Rad}^2}\frac{1}{\Lambda} \tag{9}$$

σ_{Rad} is the error in Eq. 5 which is a function of temperature shown below.

$$\sigma_{Rad} = \sqrt{32.49 + 69.7 \times 10^{-}23T_{Top}^8} \tag{10}$$

The uncertainty in the radiated power from the canister is the dominating term in Eq. 9, and this translates into an uncertainty in the lithium mass flow rate of about 0.7 mg/s at 1050 °C. The steady-state operating range of mass flow rates for lithium-fed LFA operation is between 5 and 50 mg/s.

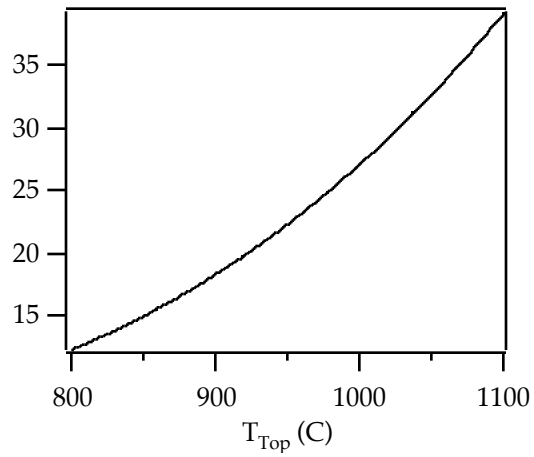

Figure 9: σ_{Rad} as a function of T_{Top}

Based on the above results an algorithm was devloped and implemented on the data monitoring computer for real-time monitoring of the mass flow rate through the thruster.

5 Conclusions

This paper documents the design, laboratory implementation and calibration of a new lithium-fed

Lorentz force accelerator (LFA). The novel concept in the design is the use of an open-ended heat pipe to supply lithium vapor through a multi-channel cathode. The device is thus free of valves and moving parts and the propellant mass flow rate is monitored and metered through water calorimetry and the power input to a furnace. Based on heat load calculations the anode was fabricated out of tungsten and has a thickness of 4.5 mm. A power balance relating the input power for the furnace vaporizing the lithium, the radiated power and the power removed by the flowing lithium vapor allowed a calibration of the mass flow rate to within 10%. The device, along with a six color video pyrometer (described in ref. [12]) and an emission spectrometer, is intended for use in the studies of various processes related to multi-channel cathodes and alkali metal plasma acclerators.

Acknowledgments The authors are thankful to Dr. Kevin Diamant for his valuabe help.

References

[1] V.P. Ageyev and V.G. Ostrovsky. High-current stationary plasma accelerator of high power. In 23^{rd} *International Electric Propulsion Conference*, Seattle, WA, USA, 1993. IEPC-93-117.

[2] J.E. Polk and T.J. Pivirotto. Alkali metal propellants for MPD thrusters. In *AIAA/NASA/OAI Conf. on Advanced SEI Technologies*, Cleveland, Ohio, 1995. AIAA-91-3572.

[3] E.Y. Choueiri and H. Okuda. Anomalous ionization in the MPD thruster. In 23^{rd} *International Electric Propulsion Conference*, Seattle, WA, USA, 1993. IEPC-93-067.

[4] V.I. Brukhty, V.N. Shutov, A.B. Smirnov, M.P. Burgasov, and A.A. Chirov. The effect of alkali metal electric rocket engines on spacecraft. In 23^{rd} *International Electric Propulsion Conference*, Seattle, WA, USA, 1993. IEPC-93-149.

[5] R.I. Samanta Roy and D.E. Hastings. Backflow contamoniation from lithium MPD thrusters: A preliminary assessment. Technical Report No. 959948, NASA-JPL Technical Report, Pasadena, CA, 1995.

[6] V.A. Petrosov, I.B. Safonov, Y.A Utkin, and V.N. Shutov. Investigation of alkali metal MPD thrusters. In 24^{th} *International Electric Propulsion Conference*, Moscow, Russia, 1995. IEPC-95-104.

[7] V. Tikhonov, S. Semenikihin, J.R. Brophy, and J.E. Polk. The experimental performance of the 100 kW lithium MPD thruster with external magnetic field. In 24^{th} *International Electric Propulsion Conference*, Moscow, Russia, 1995. IEPC-95-105.

[8] K. Goodfellow and J. Polk. Lorentz force accelrator technolgy development at JPL. In *Sixth Advanced Space Propulsion Workshop*, NASA-JPL, Pasadna, CA, 1995. pp. 129-136.

[9] F.R. Chamberlain, A.J. Kelly, and R.G. Jahn. Electropositive surface layer MPD thruster cathodes. In 25^{th} *Joint Propulsion Conference*, Monterey, CA, USA, 1989. AIAA-89-2706.

[10] J.S. Fillmore. An experimental study of lithium dispenser cathodes in the MPD thruster. In 23^{rd} *International Electric Propulsion Conference*, Seattle, WA, USA, 1993. IEPC-93-196.

[11] E.Y. Choueiri. Contributions to the Semi-Annual Progress Report for the period June 1994-December 1994. Technical Report No. EPPDyL-TR-94F, EPPDyL, Princeton University, 1994.

[12] E.Y. Choueiri, V.P. Chiravalle, G.E. Miller, and R.G. Jahn. Six-color video pyrometry with application to MPD thrusters. In 24^{th} *International Electric Propulsion Conference*, Moscow, Russia, 1995. IEPC-95-111.

[13] S.A. Semenikhin and V.B. Tikhonov. The influence of cathode design on the performance and characteristics of MPD thrusters with applied magnetic field. In 3^{rd} *Russian-German Conference on Electric Propulsion Engines and their Technical Applications*, Stuttgart, Germany, 1994. M27-M31.

[14] M. Krishnan. *Physical Processes in Hollow Cathodes in High Current Discharges*. PhD thesis, Princeton University, Princeton, NJ, USA, 1976.

[15] K.D. Diamant, E.Y. Choueiri, A.J. Kelly, and R.G. Jahn. Characterization of the near-anode region of a coaxial MPD thruster. In 30^{th} *Joint Propulsion Conference*, Indianapolis, IN, 1994. AIAA-94-3336.

[16] Roland W. Ohse. *Handbook of Thermodynamic and Transport properties of Alkali Metals*. Blackwell, New York, 1977.

[17] J.M. Prausnitz R.C. Reid and T.K. Sherwood. *The Properties of Liquids and Gases*. McGraw Hill, New York, 1977.

[18] W.B. Anderson. Porous cathode for alkali propellant mpd thrusters, quarterly report no.4, nasa sbir contract nas7-1308. Technical Report 8, Thermacore Inc., 1996.

[19] Ascher H. Shapiro. *The Dynamics and Thermodynamics of Compressible Fluid Flow*. Roland Press, New York, 1953.

[20] Frand P. Incorpera and David P. DeWitt. *Fundamentals of Heat and Mass Transfer*. John Wiley, New York, 1990.

APPENDIX: Theoretical Mass Flow Rate Prediction The mass flow rate of lithium through the thruster is influenced by two parameters, the temperature of the thruster cathode and the temperature of the canister wall during steady-state operation. The temperature of the canister wall is related to the saturation pressure of lithium vapor in the canister for temperatures around the vaporization threshold, 800°C. The temperature of the cathode surface controls the transfer of enthalpy to the lithium vapor flow through convection as the lithium moves through the channels of the cathode. A one dimensional fluid model with heat addition and friction loss was used to estimate the lithium mass flow rate as influenced by the above parameters[18].

Model Assumptions The model describes three regions of flow behavior under steady state, the conditions in the canister as a function of canister wall temperature and the flow of the lithium vapor through the vapor tube into the cathode cavity, the adiabatic expansion of the fluid as it passes from the cathode cavity into the multi-hollow-channels, and the expansion of the fluid due to friction and heat addition inside the vapor channels. The flow in all regions is considered one dimensional with no boundary layer, although boundary layer effects are introduced indirectly through friction and heat transfer coefficients. The basic equations describing the evolution of a one dimensional flow in terms of Mach number, temperature, velocity, and density are taken from Ref. [19].

The model assumes that at steady-state conditions lithium exists as a saturated vapor in the canister where the temperature of the vapor is equivalent to the temperature of the canister walls. An experimental relation between lithium vapor pressure and temperature is given in Ref. [16] and has the form below with pressure, p in Pascal.

$$p = (\frac{1}{T})^{0.4942} \exp\left(13.0719 - \frac{18880.659}{T}\right) \times 10^6 \quad (11)$$

At 1050°C, p is about 1055 Pa (8 torr) and at this low pressure the ideal gas assumption is valid. The density of the vapor can be calculated from this assumption, since the temperature is specified and the pressure is determined by Eq. 11. The state of the vapor in the canister is now completely determined. It is next assumed that the lithium vapor does not condense on the walls of the vapor tube and the flow is adiabatic as it travels into the cavity region of the cathode. Since the vapor tube is well insulated and has a small cross sectional area there is are no heat sources to supply the energy for vaporization to occur. Under steady-state conditions it is therefore expected that no net condensation takes place on the wall of the vapor tube. However it is highly probable that during the start-up phase of heater operation a surface layer of lithium is deposited on the vapor tube wall. The flow is considered incompressible as it travels between the canister and the cavity of the cathode, since a significant area contraction has not occurred. The density in the cathode cavity is taken as the density computed for the vapor in the canister. A this point in the analysis a guess is made for the mass flow rate of lithium into the cathode which is later refined through an iterative procedure. With knowledge of the cross section area of the cathode cavity, a velocity is computed and this value coupled with the stagnation temperature of the flow gives a value for the temperature of the flow in the cathode cavity. The stagnation temperature of the flow is the canister temperature.

The second region of flow behavior is the adiabatic expansion from the cavity into the vapor channels in the cathode. The area ratio between the cross section of a channel and of the entire cathode cavity is 9.97, and this value is sufficient together with the Mach number of the flow in the cavity to compute the entrance Mach number into a channel. The equations for the adiabatic expansion of a gas are given in Ref. [19]. It is further assumed that the mass flow is equally divided among the 48 channel of the porous tungsten cathode. The conditions at the channel entrance, specifically the Mach number and the temperature, are required for the next stage of the calculations.

The last stage of the algorithm determines the exit Mach number of the flow from the channel under the action of convective heat addition from the channel and of surface friction with the channel walls. It is assumed that the channel walls are all at a uniform temperature which is equal to the external surface temperature of the cathode. In general the temperature varies across the surface of the cathode, as previous studies have shown. The flow is treated as laminar flow in the channels. Ref. [16] gives an experimental expression for the viscosity of the lithium vapor, μ, shown below with μ given in kg/ms.

$$\mu = (130.6+0.1014(T-1000)+4.55\times10^{-6}(T-1000)^2)\times10^{-7} \quad (12)$$

A Reynolds number for the flow can be estimated with the canister temperature at 1050°C, by taking the density in the canister as an estimate for the density in a channel, by using the speed of sound in

lithium vapor as an estimate for the fluid velocity in a channel and by using Eq. 12 to find μ. For a channel diameter of .102 mm the Reynolds number is on the order of 100, which upholds the laminar flow approximation. Since the length of a channel is only 0.0254 m, far short of the entry length, the flow is not fully developed and the inviscid approximation is valid for the flow in the center of a channel[20]. The flow properties are calculated along the length of a channel given the initial conditions at the entrance of a channel and the temperature of the channel walls which is taken to be the cathode surface temperature as mentioned earlier. The Mach number of the flow at the exit is computed and the estimate for the total lithium mass flow is revised so that the exit Mach number is one. This choked flow assumption is valid because the pressure in the vacuum tank, into which the lithium vapor is discharged, is 10^{-5} torr which is roughly five orders of magnitude less than the lithium vapor pressure in the canister.

Numerical Method for Finding Flow Properties For the purposes of numerical integration of the fluid flow equations the channel length is partitioned into 1000 points. The fundamental equations that describe the change in the Mach number and temperature of the lithium vapor flow between the points in a channel are

$$\frac{2dM}{M} = \frac{(1+\gamma M^2)(1+\frac{\gamma-1}{2}M^2)}{1-M^2}\frac{dT_o}{T_o} + \frac{\gamma M^2(1+\frac{\gamma-1}{2}M^2)}{1-M^2}\frac{4fdx}{D} \quad (13)$$

$$\frac{dT}{T} = \frac{(1-\gamma M^2)(1+\frac{\gamma-1}{2}M^2)}{1-M^2}\frac{dT_o}{T_o} - \frac{\gamma(\gamma-1)M^4}{1-M^2}\frac{2fdx}{D}, \quad (14)$$

where dM and dT are the change in Mach number and temperature between the points x_i and $x_i + dx$ and $dx = 2.54 \times 10^{-5}$. f is the friction coefficient (Fanning) at x_i for laminar flow which is given by 16/Re, and T_o is the stagnation temperature of the flow. The stagnation temperature of the flow increases along the initial part of the channel because heat is being added to the flow. The stagnation temperature decreases as the flow reaches the channel exit because a temperature gradient favorable for heat addition from the wall is no longer present due to the effects of frictional heating in the boundary layer. The change in stagnation temperature dT_o between the points x_i and $x_i + dx$ is given by the following equation.

$$dT_o = \frac{H(T_{wall} - T_{adia})48\pi D dx}{\dot{m}_{Li} c_p} \quad (15)$$

Here T_{wall} is the channel wall temperature and H is the local heat transfer coefficient. T_{adia} is the adiabatic wall temperature and it is a measure of the temperature in the thermal boundary layer that is adjacent to the wall of the channel. T_{adia} is higher than T due to the presence of viscous heating effects in the boundary layer. It is T_{adia} that controls the direction of heat transfer from the channel wall. T_{adia} is given below.

$$T_{adia} = T(1 + 0.89\frac{\gamma-1}{2}M^2) \quad (16)$$

The coefficient 0.89 in Eq. 16 is the recovery factor and was determined from subsonic experimental data. The local heat transfer coefficient is obtained by considering laminar flow with a Nusselt number of 3.66 for a channel surface maintained at constant temperature[20]. The Nusselt number

$$Nu = \frac{HD}{\kappa}, \quad (17)$$

where κ is the lithium vapor thermal conductivity, has been measured experimentally and is given in Ref. [16]. κ is evaluated at T_{adia}.

Computational Results Following the formalism above a computer code was written in C^{++} to model the lithium mass flow rate through the thruster. A series of computations was performed to determine the mass flow rate during steady state for various canister wall temperatures, over the range of 920°C to 1100°C. In all of these calculations the temperature of the cathode was taken to be 1900 K. The results are shown in Fig. 10. It is evident from Fig. 10 that the operating range of interest for the lithium-fed LFA is between 950°C and 1070°C where the mass flow rate varies between 5 and 50 mg/s. The power required to supply lithium to the thruster at the mass flow rates calculated above was also determined using Eq. 11, the results are shown in Fig. 11. Fig. 12 shows the variation of the the Mach number along the length of a channel when the canister temperature is 1300 K and the calculated mass flow rate is 21.7 mg/s

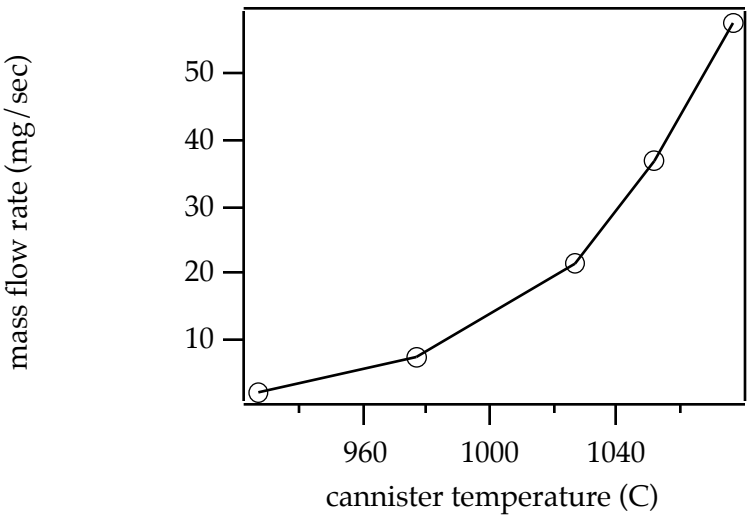

Figure 10: Model predictions for the lithium mass flow rate at several values of canister temperature

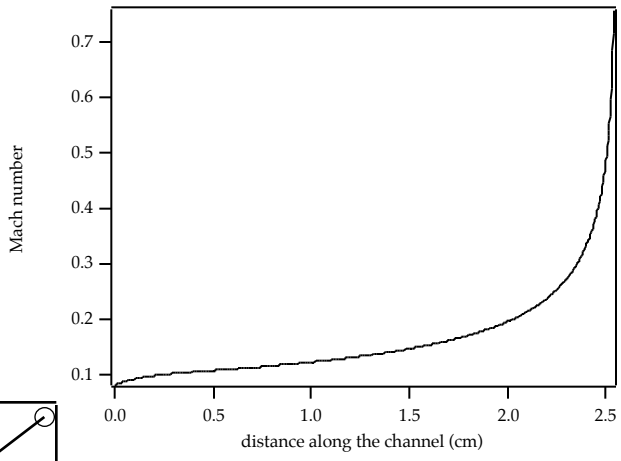

Figure 12: Calculated Mach number variation along a channel

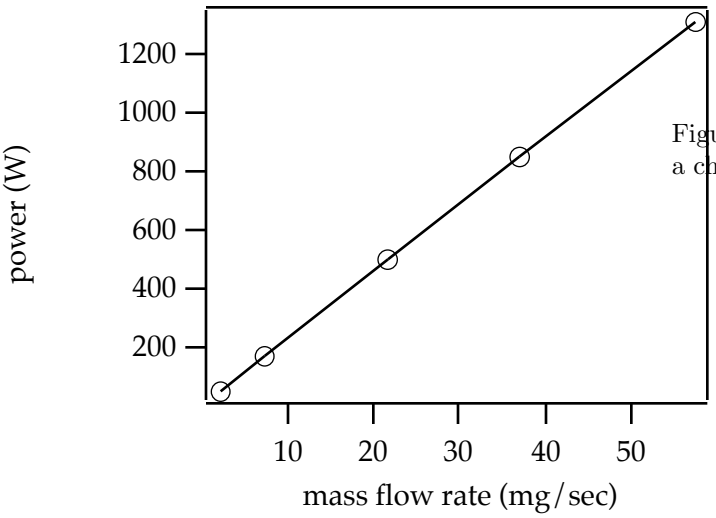

Figure 11: Calculated power required to vaporize lithium as a function of lithium mass flow rate

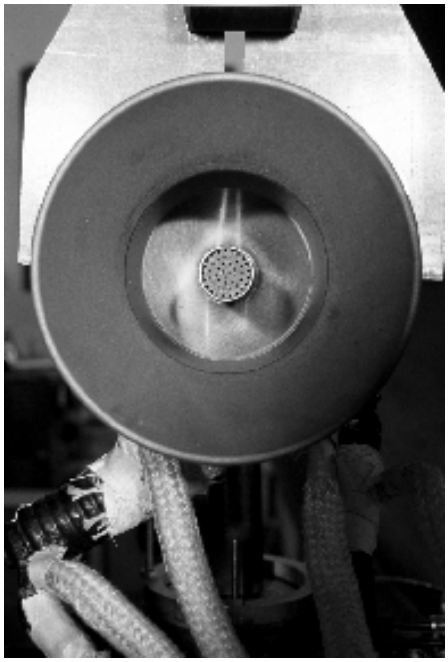

Figure 13: Close up front view. (Anode O.D.is 15 cm)

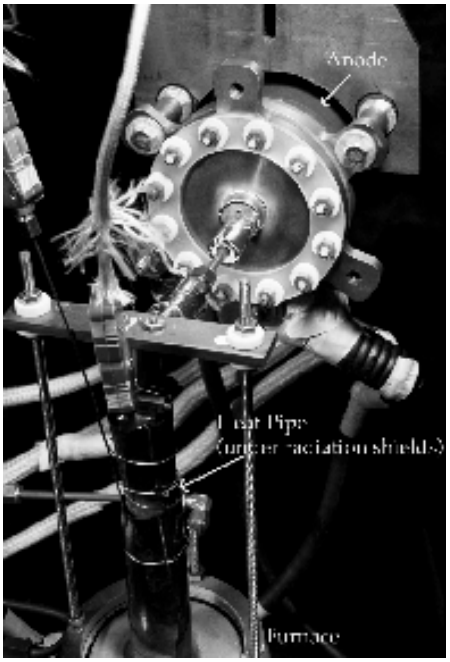

Figure 15: Close up back view showing heat pipe and thermocouples.

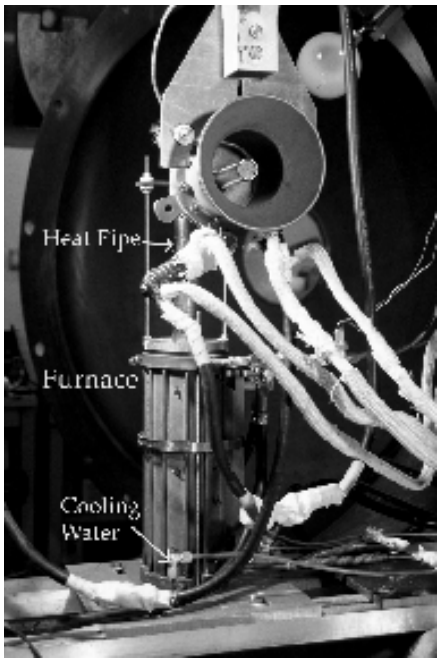

Figure 14: Front view showing furnace and electrical leads.

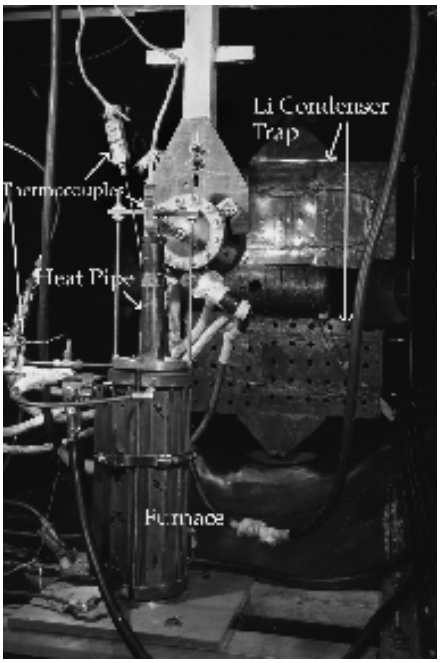

Figure 16: Back view showing water calorimetric subsystem and lithium condenser trap (downstream)